Original Article

Institution of MECHANICAL ENGINEERS
Journal of ENGINEERING TRIBOLOGY

Proc IMechE Part J:
J Engineering Tribology
0(0) 1–20

DOI: 10.1177/1350650117733374
journals.sagepub.com/home/pij
SAGE

Multi-objective optimization of stacked radial passive magnetic bearing

KP Lijesh[1], Mrityunjay Doddamani[1], SI Bekinal[2] and SM Muzakkir[3]

Abstract

Modeling, design, and optimization for performances of passive magnetic bearings (PMBs) are indispensable, as they deliver lubrication free, friction less, zero wear, and maintenance-free operations. However, single-layer PMBs has lower load-carrying capacity and stiffness necessitating development of stacked structure PMBs for maximum load and stiffness. Present work is focused on multi-objective optimization of radial PMBs to achieve maximum load-carrying capacity and stiffness in a given volume. Three-dimensional Coulombian equations are utilized for estimating load and stiffness of stacked radial PMBs. Constraints, constants, and bounds for the optimization are extracted from the available literature. Optimization is performed for force and stiffness maximization in the obtained bounds with three PMB configurations, namely (i) mono-layer, (ii) conventional (back to back), and (iii) rotational magnetized direction. The optimum dimensions required for achieving maximum load without compromising stiffness for all three configurations is investigated. For designers ease, equations to estimate the optimized values of load, stiffness, and stacked PMB variables in terms of single-layer PMB are proposed. Finally, the effectiveness of the proposed method is demonstrated by considering the PMB dimensions from the available literature.

Keywords

Magnetic bearing, conventional configuration, rotational magnetized direction configuration, multi-objective optimization

Date received: 15 June 2017; accepted: 24 August 2017

Introduction

Friction and wear are very common phenomena in components with sliding mode. Conventional roller or journal bearings are used to minimize energy losses due to friction and performance deterioration owing to wear. However, systems can further benefit from a greater reduction of friction and wear between tribo-pairs with passive magnetic bearings (PMBs) usage. These PMBs provide noncontact, maintenance-free, frictionless, and lubrication-free operations[1] due to which their implementation in applications such as molecular pumps,[2] machine tool spindles,[3] turbines,[4] flywheels,[5] control moment gyroscopes (CMG),[6] etc., has augmented. It is desirable for the PMBs to possess both higher load-carrying capacity and stiffness as far as static and dynamic performances are concerned. Figure 1(a) (Configuration 1) presents single-layer PMBs wherein polarizations of the rotor and stator magnets are same i.e. either axially or radially polarized.[7] However, such type of bearing possesses low load-carrying capacity and stiffness, which can be enhanced by stacking numbers of single-layer PMBs in the axial direction.[8,9] Two different configurations of stacked PMBs are available: (i) Configuration 2 (back to back as seen in Figure 1(b)) and (ii) Configuration 3 (rotational magnetized direction (RMD) as presented in Figure 1(c)).[10] Configuration 2 is achieved by arranging axial/radial polarized magnets back to back (Figure 1(b)), while both radially and axially polarized magnets are used to achieve Configuration 3 (Figure 1(c)). PMB are classified based on the direction of loading i.e. in axial and radial modes. Present work is focussed on bearing performance of radial PMBs.

The force and stiffness developed by a stacked radial PMBs depends on (i) the number of stack and

[1]Department of Mechanical Engineering, National Institute of Technology Karnataka, Surathkal, India
[2]Department of Mechanical Engineering, KLS Gogte Institute of Technology, Belagavi, Karnataka, India
[3]Department of Mechanical Engineering, Jamia Millia Islamia Universtiy, New Delhi,, India

Corresponding author:
KP Lijesh, Indian Institute of Technology, Hauz Khas, New Delhi 110016, India.
Email: lijesh_mech@yahoo.co.in

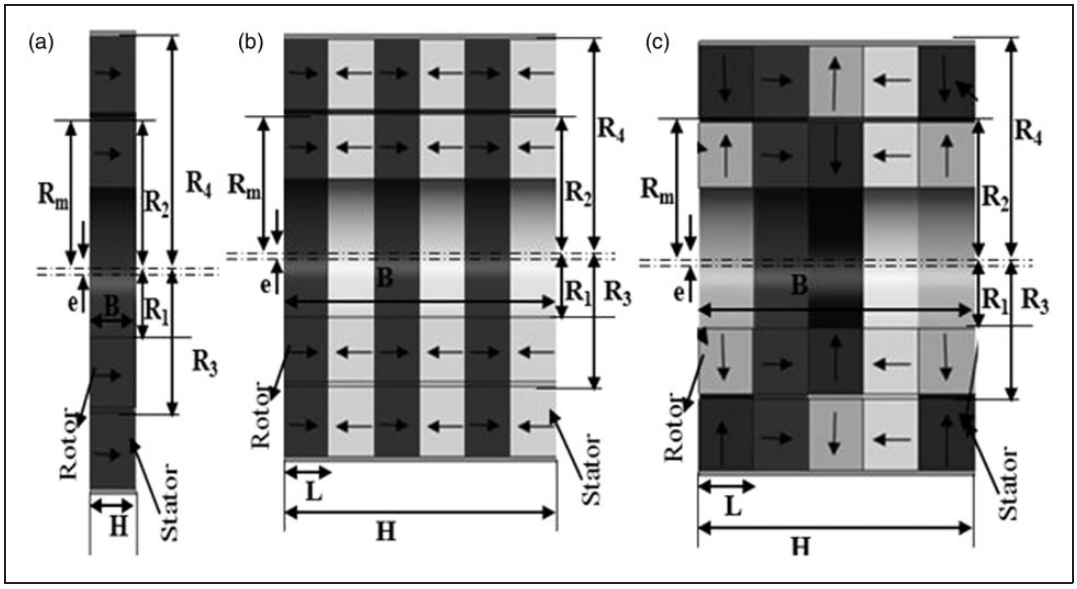

Figure 1. PMB configurations: (a) single layer, (b) conventional, (c) RMD arragments of PMB.

(ii) bearings dimension.[11] PMBs design for the given load and dynamic condition is necessary and crucial to select the optimum dimesnions and the number of stacking. Inferior design results in poor bearing performance while rugged design increases cost and volume of magnet. Therefore, the designer objective is to estimate PMB dimensions for maximizing load and stiffness. However, designing a radial PMB having both maximum radial load-carrying capacity and stiffness is complex due to its circumferncial repulsion forces. The total radial force developed by a PMB is the difference between repulsion forces by bottom half and upper half of stator magnet as depicted in Figure 2. Thereby at zero eccentricity the load-carrying capacity will be zero, since the force from the top and bottom are same. However, in case of eccentric shaft, repulsive force increases in eccentricity direction. Therefore for higher load-carrying capacity, higher clearance is envisaged.

For higher stiffness, the deflection of rotor must be less i.e. lower clearance is required. These two contradicting objectives make the design of a radial PMB quite complex. Such complications are conveniently avoided by designing radial PMBs for either maximizing load-carrying capacity or stiffness. Lijesh and Hirani[12] performed optimization of mono-layer axially polarized radial PMB, for achieving maximum load-carrying capacity while Moser et al.[11] performed optimization using finite element analysis (FEA) on the conventional stacked PMB for the maximum radial stiffness for a given control volume. Existing literature addresses design of stacked radial PMB with single objective of maximizing load or stiffness. Optimization for RMD stacked radial PMB has not been carried out yet.

Present work deals with single-objective optimizations with objective functions for (i) Case 1: Maximizing load, (ii) Case 2: Maximizing stiffness and (iii) Case 3: Minimization of volume by utilizing interior trust region optimization method. To estimate the radial load and radial stiffness of a PMB, 3D Coulombian equations[13] are adopted. To define the constraints, constants, and bounds for the optimization, the dimensions of the PMBs from available literature (inner and outer radii of rotor and stator, the axial length of rotor and stator, axial offset, and clearance)[7,10,13–19] are considered.

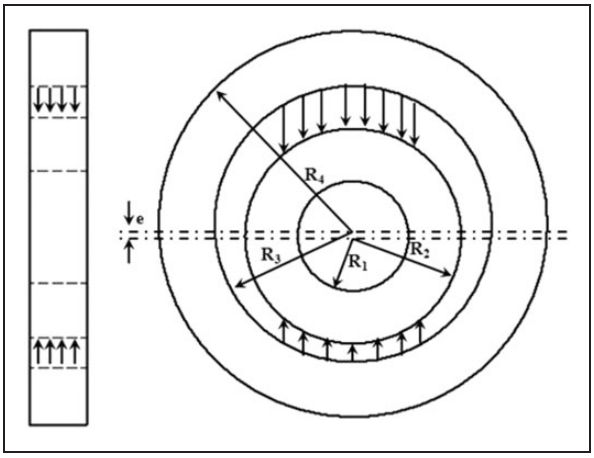

Figure 2. Single-layer passive magnetic bearing.

Optimization results reveal maximization of load lead to stiffness reduction and vice versa. These observations necessitate the authors to perform a multi-objective optimization on all three enlisted PMB configurations for achieving maximum radial load and stiffness. The obtained results are compared with first objectives values. The optimization is extended for different outer radii and volumes. For each case, load and stiffness variation with stacking number is proposed in equations form. Further, equations for estimating mean radius, clearance, axial length, and inner radius with respect to stacking number for

achieving both maximum load and stiffness are provided. Finally, to validate and demonstrate the effectiveness of the present approach, dimensions of stacked PMBs from a published literature are considered and results and elaborate discussion on findings are presented.

Mathematical modeling

Three-dimensional Coulombian equations used for estimating the radial load for (i) Configuration 1: Single-layer PMB (Figure 1(a)), (ii) Configuration 2: Conventional back-to-back PMB (Figure 1(b)), and (iii) Configuration 3: RMD (Figure 1(c)) PMBs is described herewith. Further, details of the optimization method along with their bounds and constants are also detailed.

Mathematical modeling of passive magnetic bearing configurations

The equation used in the present work for estimating the radial force ($F_{y,a}$) exerted by axially polarized outer ring magnet on the inner one is presented in the following equation (1)[16]

$$F_{y,a} = \frac{Br_1 Br_2}{4\pi\mu_0}\left(R(z_a) + R(z_a + H - B) + R(z_a + H) + R(z_a - B)\right) \quad (1)$$

where $R(\alpha)$ is given by

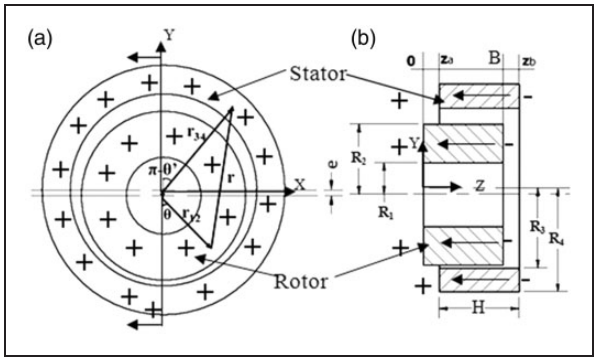

Figure 3. Configuration 1: coordinates of single-layer magnetic bearing: (a) front view, (b) sectional side view.

value is estimated using the following equation and is given by

$$K_y = \frac{dF_{y,a}}{de} \quad (3)$$

The 3D Coulombian equations used for Configurations 2 and 3 are presented in equations (4) and (5), respectively. Details of the derivation of these equations are provided by Lijesh and Hirani.[18]

$$F_{y,CON} = \sum\left(\sum_{j=1}^{k} F_{y,a,j}\right) \quad (4)$$

$$F_{y,RMD} = \sum\left(\sum_{j=1}^{k} F_{y,a,i,j} + \sum_{j=1}^{m} F_{y,p,i,j}\right) \quad (5)$$

$$R(\alpha) = \int_0^{2\pi}\int_0^{2\pi}\int_{R_3}^{R_4}\int_{R_1}^{R_2}\left[\frac{(e + r_{12}\cos(\theta) - r_{34}\cos(\theta'))r_{12}r_{34}}{\left(r_{12}^2 + r_{34}^2 + e^2 - 2r_{12}r_{34}\cos(\theta - \theta') + 2e(r_{12}\cos(\theta) - r_{34}\cos(\theta')) + (\alpha)^2\right)^{1.5}}\mathrm{d}r_{12}\mathrm{d}r_{34}\mathrm{d}\theta\mathrm{d}\theta'\right] \quad (2)$$

where R_1 and R_2 is the inner and outer radius of the rotor magnet and R_3 and R_4 is the inner and outer radius of the stator magnet, respectively (Figure 3(b)). Eccentricity "e" is between the rotor and stator magnet while H and B represents the axial lengths of the stator and rotor magnets, respectively. The value of θ varies from "θ_1=0" and "θ_2=2π" for full ring rotor and value of θ varies from "θ_3=0" and "θ_4=2π" for a full ring stator magnet. Stiffness

where k is the number of pairs of axially polarized ring magnets and m is the number of pairs of perpendicularly polarized ring magnets in RMD configuration. Perpendicular (radial) force in "Y" direction is given by the following equation

$$F_{y,p} = \frac{Br_1 Br_2}{4\pi\mu_0}\left(A(z_a, R_1) - A(z_a + H, R_1) - A(z_a, R_2) + R(z_a + H, R_2)\right) \quad (6)$$

where

$$A(z_a, R_1) = \int_0^{2\pi}\int_0^{2\pi}\int_0^{L}\int_{R_3}^{R_4}\frac{(e + R_1\cos(\theta) - r_{34}\cos(\theta'))}{\left(R_1^2 + r_{34}^2 + e^2 - 2R_1 r_{34}\cos(\theta - \theta') + 2e(R_1\cos(\theta) - r_{34}\cos(\theta')) + (z_a - z_{34})^2\right)}\mathrm{d}r_{34}\mathrm{d}z_{ab}\mathrm{d}\theta\mathrm{d}\theta' \quad (7)$$

Optimization

In the present work, optimization will be performed by considering single and multi-objective functions. Single-objective optimization is performed for (i) maximizing force, (ii) maximizing stiffness, and (iii) minimizing volume. In each case, the variation in values of load, stiffness, volume, and variables is discussed and detailed. Multi-objective optimization is performed by considering both stiffness and force in single-objective function with constant volume. Further, the importance of considering multi-objective optimization for stacked PMBs is demonstrated.

Single-objective optimization

For performing optimization, it is necessary to define objective functions, variables, constants, and constraints. For this, inner radius of the rotor (R_1), axial length of the rotor (H), clearance (C), axial offset (z_0), outer radius of rotor (R_4), and mean radius (R_m) are considered as variables. The optimization is performed by considering a single value of eccentricity ratio (ε)=0.9 and remanence values of rotor (Br_1) and stator (Br_2) magnets as 1T. Bounds and constant values for the present work is selected from relevant available literature[7,10,13–20] and the extracted bound values are: R_1=0.002–0.022 m, H=0.003–0.05 m, C=0.001–0.005 m, R_m = 0.0145–0.047 m, z_0=0–0.001 m, and R_4=0.01–0.05 m. The rounded off bound values are R_1=0.002–0.025 m, H=0.003–0.05 m, C=0.0005–0.005 m, R_4=0.01–0.05 m, and z_0=0–0.0011 m. The constraints, bounds, and constants considered for the optimization are consolidated as follows

Constraints:

$$R_m = \frac{R_2 + R_3}{2} \tag{8}$$

$$R_4 > R_m + 0.5C \tag{9}$$

Bounds: $[\mathrm{H}, \mathrm{R}_1, \mathrm{R}_\mathrm{m}, R_4, \mathrm{C}, \mathrm{z}_\mathrm{a}]$

$$\begin{aligned} &\textit{Minimum Bound} \\ &= [0.003, 0.002, 0.003, 0.010.0005, 0] \\ &\textit{Maximum Bound} \\ &= [0.05, 0.02, 0.055, 0.05, 0.005, 0.0011] \end{aligned}$$

Constants:

$$Br_1 = Br_2 = 1\ T, \varepsilon = 0.9$$

As mentioned earlier, optimzation will be performed considering different cases of single-objective functions (i) Case 1: Maximizing force, (ii) Case 2: Maximizing stiffness, and (iii) Case 3: Minimizing volume, for Configuration 1. For Case 1 and Case 2, equations (1) and (3) are maximized respectively, while for Case 3, equation (10) is minimized

$$Vol. = \pi H\left(\left(R_2^2 - R_1^2\right) + \left(R_4^2 - R_3^2\right)\right) \tag{10}$$

Multi-objective optimization

Multi-objective optimization can be performed in two ways as:

(i) *Priori articulation of preferences:* In this approach, multiple numbers of individual objective functions with pre-defined weight factors are merged into a single utility function. Equation is solved as a single-objective optimization problem. Weight factors articulate the relative importance of objective function in the overall utility measure. Advantage of this approach is that it will yield a single solution depending on the weightage provided in the objective function.
(ii) *Posteriori articulation of preferences:* In this approach, a number of noninferior (a set of equally efficient) solutions are generated and then final decision is made on any one solution. This approach is often referred to as Pareto optimal approach.

Since the later approach yields multiple solutions leading towards difficulty for comparison, former approach is followed in the present work. For this, a proposed objective function involving both stiffness and force is presented in equation (11). In equation (11), *Fun* is the objective function, F_x and K_x will be the estimated optimum force and stiffness while F_n and K_n is the estimated nth force and stiffness values for Case 1 and Case 2 respectively

$$Fun = 1 - 0.5\left(\frac{F_x}{F_n}\right) - 0.5\left(\frac{K_x}{K_n}\right) \tag{11}$$

In both cases, optimization is performed using minimizing function *fmincon* and interior-region method using MATLAB. This method has proved to be very successful in solving large linear and nonlinear programming problems,[20] hence adopted for current investigations.

Results and discussions

Outcome of single-objective optimization for all three cases i.e. load, stiffness, and volume along with the values of variables for Configuration 1 are presented in Table 1.

Comparing the load and stiffness values of Case 1 and Case 2 from Table 1, it can be concluded that the optimization performed for maximizing load (Case 1) will lead to minimization of stiffness values and vice

Table 1. Optimization results of Configuration 1 for different objectives of optimization.

Case	Load (N)	Stiffness (N/m)	Vol. (m^3)	H (m)	R_1 (m)	R_m (m)	R_4 (m)	C (m)	z_a (m)
1	97	27,771	2.15×10^{-4}	0.0319	0.001	0.0357	0.05	0.005	0
2	31.6	70,259	8.84×10^{-5}	0.016	0.0264	0.0425	0.05	0.0005	0
3	21.9	6260	1.48×10^{-7}	0.0038	0.0409	0.0419	0.05	0.0039	0

Table 2. Optimization results of Configuration 2 for Case 1 for maximizing load.

n	Load (N)	Stiffness (N/m)	Vol. ($\times 10^{-6} m^3$)	L (m)	H (m)	R_1 (m)	R_m (m)	R_4 (m)	C (m)	z_a (m)
2	236	45,933	327	0.025	0.05	0.001	0.0346	0.05	0.005	0
3	333	74,182	336	0.0167	0.05	0.001	0.0361	0.05	0.005	0
4	394	87,632	334	0.0125	0.05	0.001	0.037	0.05	0.005	0
5	433	97,823	334	0.01	0.05	0.001	0.0378	0.05	0.0049	0
6	460	118,060	338	0.0083	0.05	0.001	0.039	0.05	0.0043	0
7	482	141,200	343	0.0071	0.05	0.001	0.04	0.05	0.0038	0
8	500	162,880	352	0.0063	0.05	0.001	0.0407	0.05	0.0034	0
9	514	184,220	355	0.0056	0.05	0.001	0.0413	0.05	0.0031	0
10	527	209,470	355	0.005	0.05	0.001	0.042	0.05	0.0028	0

Table 3. Optimization results of Configuration 2 for Case 2 for maximizing stiffness.

n	Load (N)	Stiffness (N/m)	Vol. ($\times 10^{-6} m^3$)	L (m)	H (m)	R1 (m)	Rm (m)	R4 (m)	C (m)	za (m)
2	63.4	140,580	298	0.025	0.05	0.0253	0.0425	0.05	0.0005	0
3	94	210,830	282	0.0167	0.05	0.0257	0.0425	0.05	0.0005	0
4	125.7	279,540	259	0.0125	0.05	0.0284	0.0429	0.05	0.0005	0
5	156	347,010	246	0.01	0.05	0.0285	0.0435	0.05	0.0005	0
6	184	415,380	225	0.0083	0.05	0.032	0.0434	0.05	0.0005	0
7	210	487,650	215	0.0071	0.05	0.033	0.0434	0.05	0.0005	0
8	235	562,550	200	0.0063	0.05	0.0339	0.0435	0.05	0.0005	0
9	260	628,870	192	0.0056	0.05	0.0351	0.0441	0.05	0.0005	0
10	280	703,470	186	0.005	0.05	0.0329	0.0444	0.05	0.0005	0

versa owing to clearance values. Higher clearance is required for achieving higher load-carrying capacity while lower values necessitate higher stiffness. Further, from Case 3 it can be inferred that, the reduction in volume has lead to decrease in both load and stiffness values and this is mainly due to the considerable reduction in the axial length value. Other observations of the results (Table 1) are:

1. For achieving maximum load-carrying capacity, the value of outer radius of stator and clearance has to be maximum while inner radius of rotor and axial offset must be minimum. However, axial length and mean radius are found to be neither maximum nor minimum.
2. For attaining higher stiffness, axial offset and clearance has to be minimum. While inner and outer radius of rotor is maximum. The axial length and mean radius is an intermediate value and are different from Case 1.
3. For achieving minimum volume, axial length of PMB has to be minimized.

In the second phase of the work, focus is on understanding the variation of the loads, stiffness and other variables values of Configuration 2 for Cases 1 and 2. Methodology adopted earlier is used and results for Case 1 and Case 2 are tabulated in Tables 2 and 3 and graphed in Figure 4(a) and (b), respectively.

For Case 1 (Figure 4(a)), increase in stiffness is observed to be linear with the number of stacking;

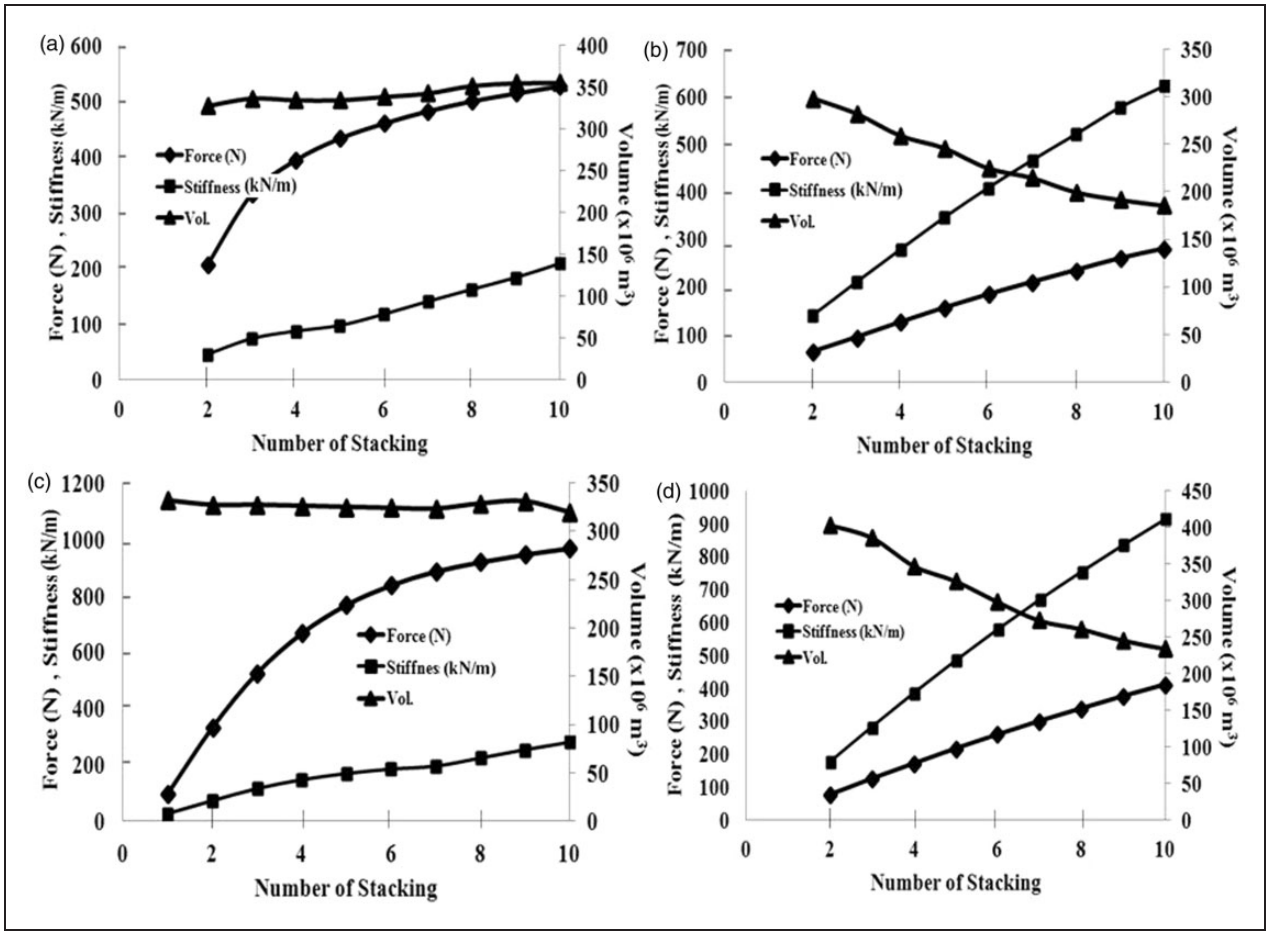

Figure 4. Plot of force, stiffness and volume for Configurations 2 and 3: (a) Configuration 2: Case 1 (max. load), (b) Configuration 2: Case 2 (max. stiffness), (c) Configuration 3: Case 1 (max. load), (d) Configuration 3: Case 2 (max. stiffness).

however, the increase in load is found to be nonlinear. Volume is found to be constant. Further from Table 2, it can be observed that the values of axial length (H), inner radius of rotor (R_1), outer radius of stator (R_4), and axial offset (z_0) are constant with the number of stacking. However, the values of mean radius (R_m) increased and clearance values (C) reduced with the number of stacking.

For Case 2 (Figure 4(b)), linear increase of force and stiffness, and decrease in volume with the number of stacking is observed. From Table 3, it can be observed that the values of axial length (H), clearance (C), outer radius of stator (R_4), and axial offset (z_a) are constant with the number of stacking. However, the values of mean radius (R_m) and inner radius of rotor (R_1) increased with the number of stacking, while the increase of mean radius values for Case 2 is very less compared to Case 1.

In the third phase of the work, the above calculation is performed for Configuration 3 and the obtained results for Case 1 and Case 2 are tabulated in Tables 4 and 5 and in Figure 4(c) and (d), respectively. Comparing Figure 4(a) and (b) and Figure 4(c) and (d) it can be concluded that the pattern of variation of load, stiffness, and volume with the number of stacking is similar for Configurations 2 and 3; however, the magnitude of load and stiffness values are higher for Configuration 3. The values of variable H, R_1, R_4, C, and z_a are almost constant for Case 1, while the values of R_m increased with the number of stacking. For Case 2, the values of R_m and R_1 increased with the number of stacking, while the values of other variables remained constant.

An attempt is made to represent the variation of load and stiffness with respect to the number of stacking in the form of an equation, for both cases and configurations. From Table 3 and Figure 5(a), the variation of stiffness values with the number of stacking for Configuration 2 and Case 2 is found to be directly proportional i.e. $K_n = nK_r$. Here, n is the number of stacking, K_n is the stiffness value of the nth stacking, and K_r is the stiffness value of single ring pair PMB. Similarly, the variation of stiffness with "n" for Configuration 3 and Case 2 is found to be $K_n = 1.3(nK_r)$. Therefore, it can be concluded that the stiffness value is increased by 1.3 times for Configuration 3 (RMD) compared to Configuration 2. The obtained value of stiffness from optimization and the values obtained from the estimated fitness equation for both configurations are plotted in Figure 5(a).

Table 4. Optimization results of Configuration 3 for Case 1 for maximizing load.

n	Load (N)	Stiffness (N/m)	Vol. ($\times 10^{-6}$ m^3)	L (m)	H (m)	R_1 (m)	R_m (m)	R_4 (m)	C (m)	z_a (m)
2	432	73,931	328	0.025	0.05	0.001	0.041	0.05	0.005	0
3	585	116,890	328	0.0167	0.05	0.001	0.041	0.05	0.005	0
4	686	148,080	327	0.0125	0.05	0.001	0.0417	0.05	0.005	0
5	767	170,460	326	0.01	0.05	0.001	0.0425	0.05	0.005	0
6	837	186,160	325	0.0083	0.05	0.001	0.0431	0.05	0.005	0
7	886	196,940	324	0.0071	0.05	0.001	0.0437	0.05	0.005	0
8	919	225,510	330	0.0063	0.05	0.001	0.0443	0.05	0.005	0
9	946	255,100	332	0.0056	0.05	0.001	0.0447	0.05	0.005	0
10	968	281,500	320	0.005	0.05	0.001	0.0451	0.05	0.005	0

Table 5. Optimization results of Configuration 3 for Case 2 for maximizing stiffness.

n	Load (N)	Stiffness (N/m)	Vol. ($\times 10^{-6}$ m^3)	L (m)	H (m)	R1 (m)	Rm (m)	R4 (m)	C (m)	za (m)
2	79	175,760	392.69	0.025	0.05	0.0039	0.0437	0.05	0.0005	0
3	127	282,370	385.5	0.0167	0.05	0.0012	0.0443	0.05	0.0005	0
4	173	365,380	347.1	0.0125	0.05	0.0157	0.0449	0.05	0.0005	0
5	218	454,450	326.38	0.01	0.05	0.0194	0.0454	0.05	0.0005	0
6	260	539,110	298.22	0.0083	0.05	0.0236	0.0458	0.05	0.0005	0
7	301	639,390	272.73	0.0071	0.05	0.0268	0.0461	0.05	0.0005	0
8	339	734,650	261.09	0.0063	0.05	0.0281	0.0464	0.05	0.0005	0
9	376	836,550	245.53	0.0056	0.05	0.0298	0.0466	0.05	0.0005	0
10	411	914,710	234.18	0.005	0.05	0.031	0.0468	0.05	0.0005	0

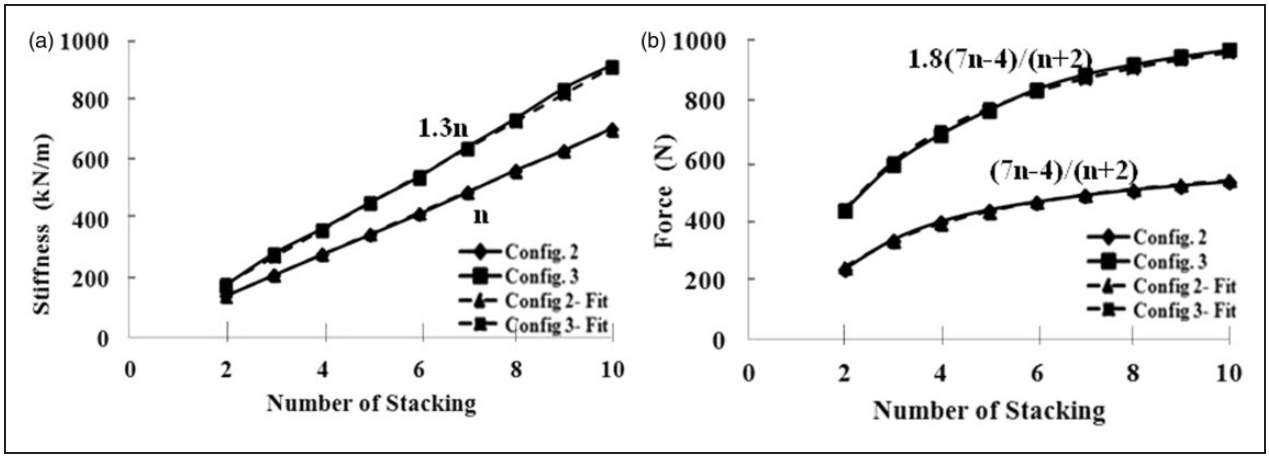

Figure 5. Estimated values from optimization and curve fitting equations of force and stiffness for Configurations 2 and 3: (a) stiffness, (b) force.

For Configuration 2 and Case 1, the variation of load with the number of stacking (n) is estimated to be F_n=[(7n-4)/(n+2)]F_r. F_n is the force provided by n stacking and F_r is the force by single ring pair PMB. For Configuration 3, the estimated load variation with "n" is F_n=[1.8(7n-4)/(n+2)]F_r. Therefore, it can be concluded that the load-carrying capacity of PMB can be increased by 1.8 times of Configuration 2, by using Configuration 3. The values of load estimated from optimization along with the values obtained from fitness equation are depicted in Figure 5(b). Optimization performed for maximizing force will lead to minimization of stiffness and vice versa and its due to the clearance value. However, a combined contribution of the stiffness and load is required for the efficient and effective PMB working. Therefore, in

Table 6. Multi-objective optimization results of Configuration 2 for given volume $1.5 \times 10^{-4}\,m^3$.

n	Load (N)	Stiffness (kN/m)	Vol. $\times 10^{-6}\ m^3$)	L (m)	H (m)	R_1 (m)	R_m (m)	R_4 (m)	C (m)	z_0 (m)
1	78	44.9	150	0.0204	0.0204	0.001	0.04	0.05	0.002	0
2	116	86.607	150	0.0101	0.0202	0.025	0.041	0.05	0.0017	0
3	159	136.05	150	0.0102	0.0306	0.0285	0.0416	0.05	0.0015	0
4	200	183.09	150	0.0086	0.0344	0.0316	0.0425	0.05	0.0013	0
5	234	233.57	150	0.0076	0.038	0.0337	0.0432	0.05	0.0012	0
6	271	277.48	150	0.0068	0.0408	0.0351	0.0436	0.05	0.0011	0
7	301	320.86	150	0.0062	0.0434	0.0362	0.044	0.05	0.0011	0
8	338	364.11	150	0.0058	0.0464	0.0371	0.0443	0.05	0.001	0
9	371	412.05	150	0.0054	0.0486	0.0379	0.0446	0.05	0.001	0
10	410	450.41	150	0.005	0.05	0.0386	0.0448	0.05	0.0009	0

Table 7. Multi-objective optimization results of Configuration 3 for given volume $1.5 \times 10^{-4}\,m^3$.

n	Load (N)	Stiffness (N/m)	Vol. ($\times 10^{-6}\ m^3$)	L (m)	H (m)	R_1 (m)	R_m (m)	R_4 (m)	C (m)	z_0 (m)
2	174	120.57	150	0.0123	0.0246	0.022	0.0426	0.05	0.0016	0
3	240	177.12	150	0.0098	0.0294	0.0249	0.0438	0.05	0.002	0
4	310	228.25	150	0.0084	0.0336	0.02651	0.0446	0.05	0.0018	0
5	368	301.19	150	0.0073	0.0365	0.029	0.0453	0.05	0.0015	0
6	428	361.22	150	0.0065	0.039	0.032	0.0458	0.05	0.0012	0
7	495	419.94	150	0.0061	0.0427	0.0344	0.046	0.05	0.0013	0
8	561	473.81	150	0.0057	0.0456	0.0368	0.0463	0.05	0.0012	0
9	616	535.28	150	0.0052	0.0468	0.0374	0.0443	0.05	0.0011	0
10	670	596.262	150	0.0045	0.045	0.0387	0.0452	0.05	0.0011	0

the subsequent section, optimization will be performed considering force and stiffness maximization. However, the optimization for minimization of volume did not provide any useful information thereby the optimization will be performed considering constant volume. Multi-objective optimization is conducted for minimization of equation (11) with constant volume. Average volume of Cases 1 and 2 for Configuration 1 i.e. $1.5 \times 10^{-4}\,m^3$ is considered. The obtained results for Configurations 2 and 3 are presented in Tables 6 and 7, respectively.

The variation of stiffness values with the number of stacking for both configurations are found to be same as the earlier case, i.e. for Configuration 2 the estimated equation fitting the estimated optimization values are $K_n = nK_r$ and for Configuration 3 is $K_n = 1.3nK_r$. The obtained values of stiffness from optimization and fitness equation are plotted in Figure 6(b). The load-carrying capacity obtained from optimization is linear and the trend is not the same as that obtained in single-objective optimizations. The obtained equations fitting the estimated optimization values for Configuration 2 is $F_n = (0.45n + 0.85)F_r$ and for Configuration 3 is $F_n = 1.5(0.45n + 0.85)F_r$. The obtained values from the fitting equation for load and stiffness is plotted in Figure 6(a) and (b), respectively. It can be inferred that by using RMD configuration (Configuration 3), the force and stiffness values increased by 1.3 and 1.5 times respectively, compared to conventional stacking arrangement (Configuration 2). Irrespective of the single or multiple objective function optimizations, the variation of stiffness with "n" is same at different load values as seen from the prevailing discussions.

Multi-objective optimization considering different R_4/H values

Prevailing methodology is repeated for $R_4/H = 1.25$ and $R_4/H = 0.75$ to understand the variation of force and stiffness values. Equations fitting the estimated values of stiffness and force from optimization are found. The optimization was performed considering equation (11) as the objective function and the obtained values for Configurations 2 and 3, after performing optimization for $R_4/H = 1.25$ and are tabulated in Tables 8 and 9, respectively. It is observed that the equation fitting the values for stiffness for both configurations for $R_4/H = 1.25$ is same as that of $R_4/H = 1$, while it is different for load.

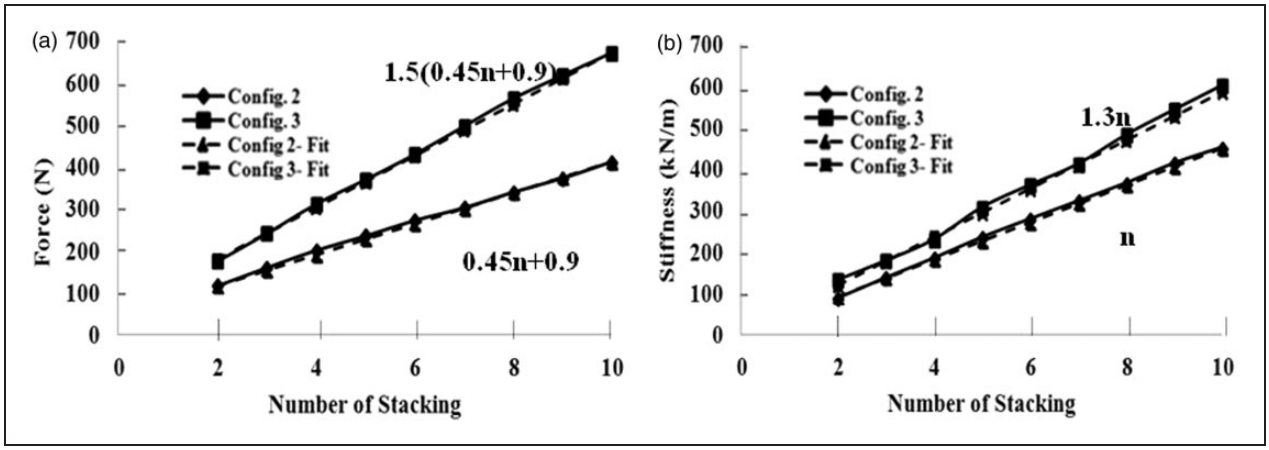

Figure 6. Plot of force and stiffness for Configurations 2 and 3 considering multi-objective optimization: (a) force vs. *n*, (b) stiffness vs. *n*.

Table 8. Optimization results of Configuration 2 considering $R_4/H = 1.25$.

n	Load (N)	Stiffness (kN/m)	Vol. ($\times 10^{-6}$ m^3)	*L* (m)	*H* (m)	R_1 (m)	R_m (m)	R_4 (m)	*C* (m)	z_0 (m)
1	93	60,340	150	0.0204	0.0126	0.018	0.0514	0.0625	0.0021	0
2	165	121,850	150	0.0126	0.0184	0.0222	0.0525	0.0625	0.0017	0
3	204	179,640	150	0.0102	0.0223	0.0257	0.0534	0.0625	0.0015	0
4	250	243,520	150	0.0086	0.0264	0.0278	0.0547	0.0625	0.00135	0
5	276	299,640	150	0.0076	0.03	0.0298	0.0557	0.0625	0.0012	0
6	319	363,898	150	0.0068	0.0324	0.0316	0.056	0.0625	0.00115	0
7	354	421,560	150	0.0062	0.0351	0.0323	0.0568	0.0625	0.0011	0
8	390	485,750	150	0.0058	0.038	0.0336	0.0575	0.0625	0.00105	0
9	425	548,523	150	0.0054	0.0414	0.0347	0.0575	0.0625	0.001	0
10	454	607,600	150	0.005	0.044	0.0358	0.0578	0.0625	0.00095	0

Table 9. Optimization results of Configuration 3 considering R4/H = 1.25.

n	Load (N)	Stiffness (N/m)	Vol. ($\times 10^{-6}$ m^3)	*L* (m)	*H* (m)	R_1 (m)	R_m (m)	R_4 (m)	*C* (m)	z_0 (m)
2	248	131,110	150	0.0123	0.0246	0.0204	0.0426	0.0625	0.0017	0
3	355	205,620	150	0.0098	0.0294	0.0243	0.0438	0.0625	0.0016	0
4	458	283,880	150	0.0084	0.0336	0.0275	0.0446	0.0625	0.0015	0
5	508	363,360	150	0.0073	0.0365	0.0295	0.0453	0.0625	0.0015	0
6	595	444,840	150	0.0067	0.04	0.0324	0.0458	0.0625	0.0014	0
7	624	527,210	150	0.0061	0.0427	0.0335	0.0463	0.0625	0.0013	0
8	672	611,820	150	0.0057	0.0456	0.0358	0.0468	0.0625	0.0012	0
9	715	699,210	150	0.0053	0.0478	0.0363	0.0475	0.0625	0.0011	0
10	757	785,830	150	0.005	0.05	0.0369	0.0482	0.0625	0.0011	0

The equation fitting the load values for Configuration 2 and Configuration 3 is $F_n = (0.45n + 0.9)F_r$ and $F_n = 1.65(0.45n + 0.9)F_r$, respectively. The obtained values from the optimization and estimated values from curve fitting equation for load and stiffness are plotted in Figure 7(a) and (b), respectively.

The obtained optimized values for Configurations 2 and 3 for $R_4/H = 0.75$ is plotted in Figure 7(c) and (d), respectively. The equation fitting the estimated values of stiffness from optimization is same as that of $R_4/H = 1$ and $R_4/H = 1.25$ and also the primary equation $(0.45n + 0.9)$ fitting the estimated load

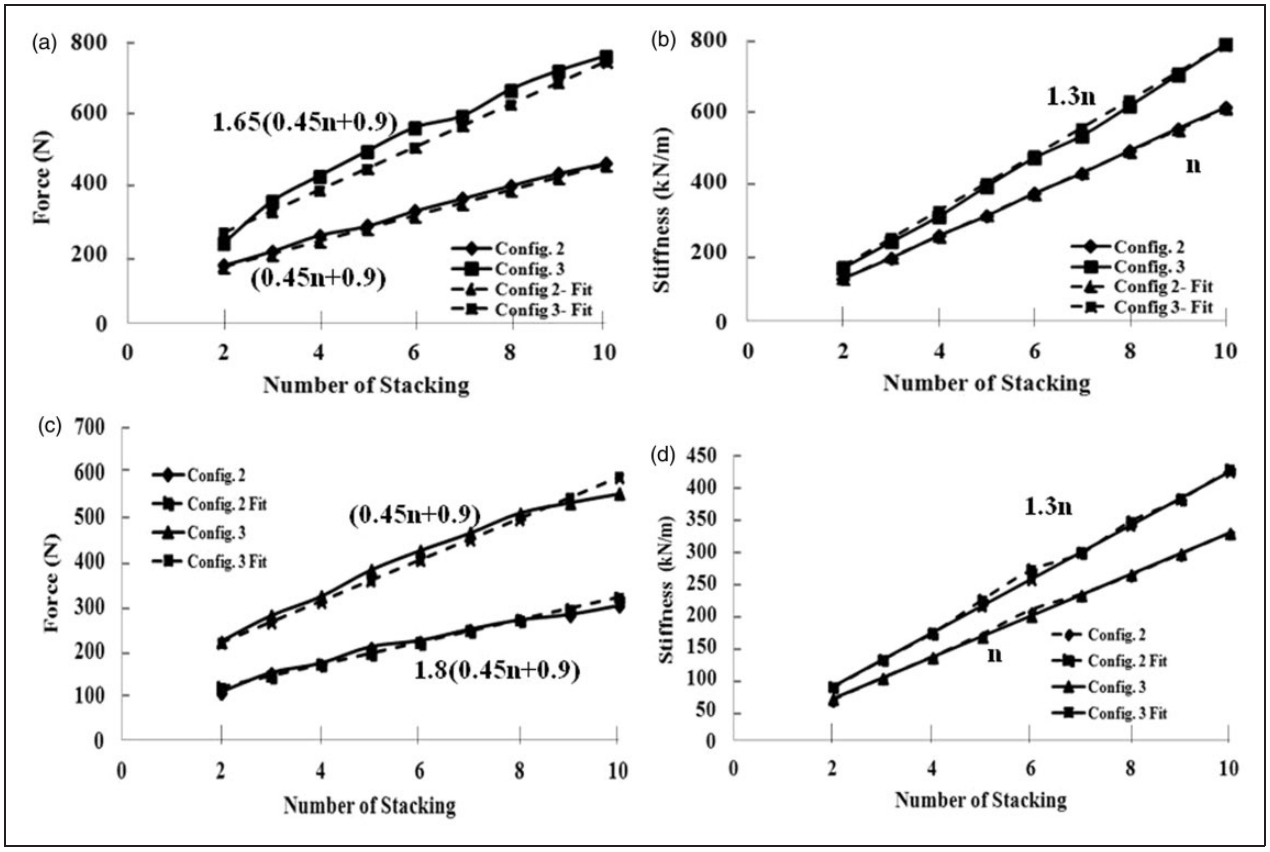

Figure 7. Force and stiffness of Configurations 2 and 3 for different R_4/H values and same $V=1.5\times10^{-4}$ m^3: (a) force vs. n for $R_4/H=1.25$, (b) stiffness vs. n for $R_4/H=1.25$, (c) force vs. n for $R_4/H=0.75$, (d) stiffness vs. n for $R_4/H=0.75$

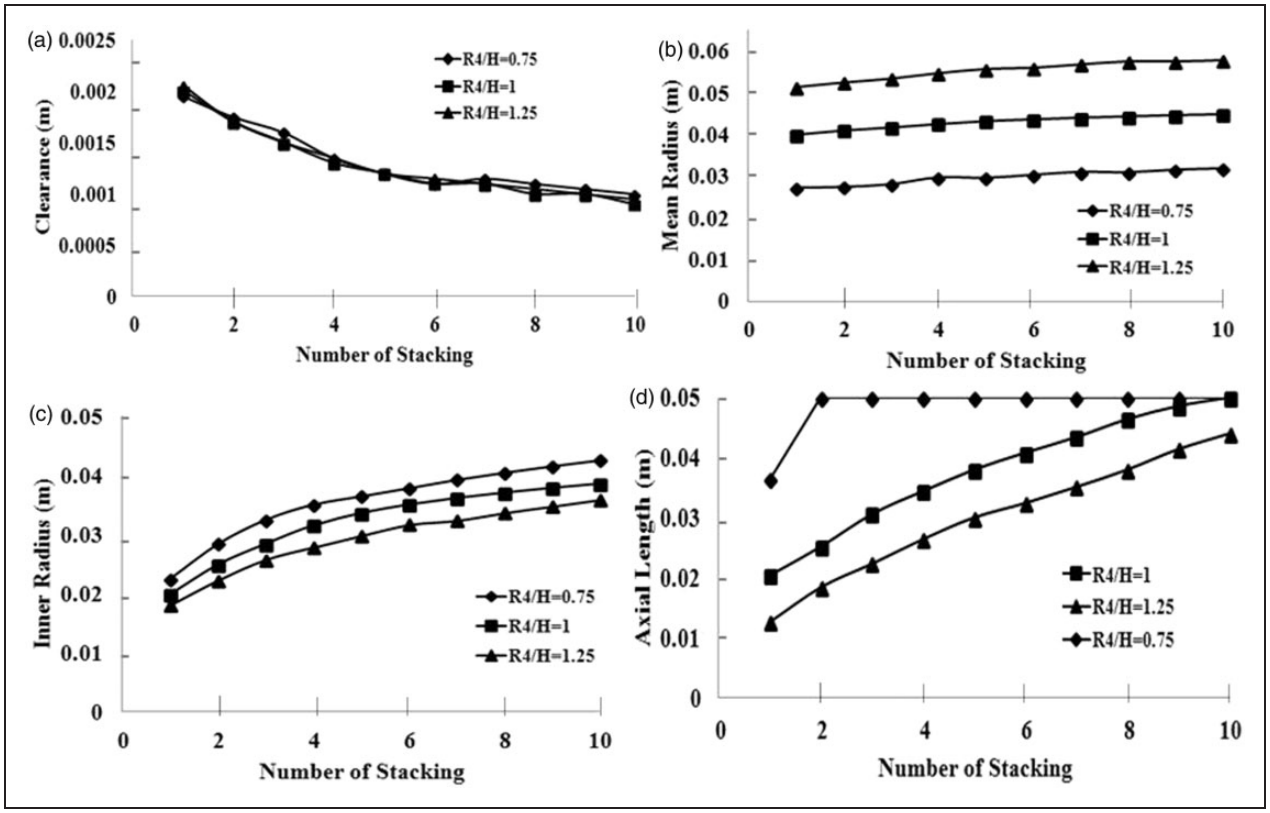

Figure 8. Variation in parameters with number of stacking of Configuration 2 for different R_4/H values: (a) clearance, (b) mean radius, (c) inner radius, (d) axial length.

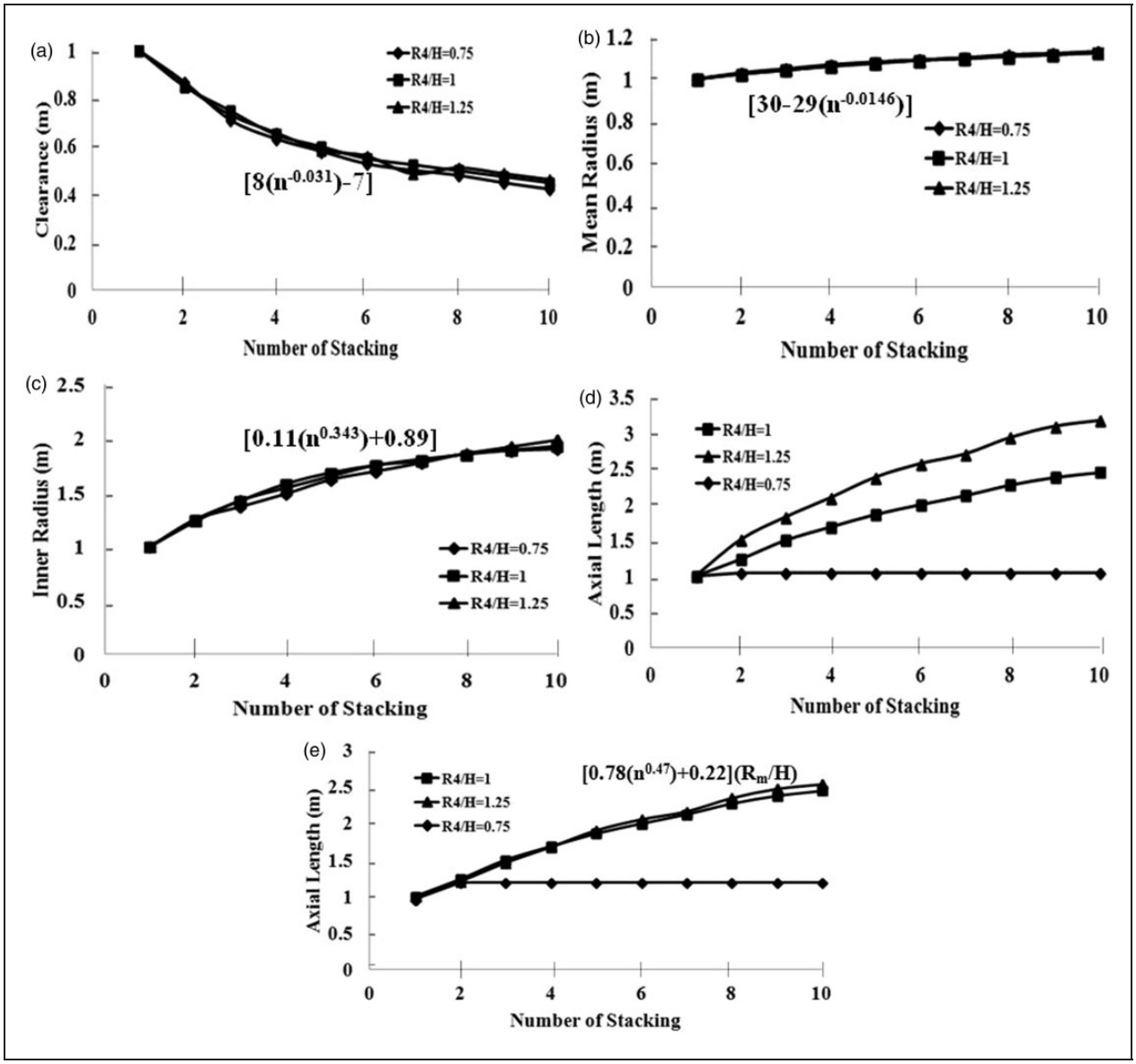

Figure 9. Variation of variables with the number of stacking and curve fit equation of Configuration 2 for different R_4/H values: (a) clearance, (b) mean radius, (c) inner radius, (d) axial length, (e) modified variation of axial length with n.

values are also found to be the same. However, the increase in load values between the configurations is different. The equation fitting the load values for Configurations 2 and 3 is $F_n = 1.8(0.45n+0.9)F_r$ and $F_n = (0.45n + 0.9)F_r$. The estimated values from the predicted curve fit equation for load and stiffness is plotted in Figure 7(c) and (d), respectively. From the above discussion, it can be concluded that the variation of stiffness for different numbers of stacking is same for different R_4/H values; however, it is different for the case of load. In the following section, understanding of the variations of variables C, R_m, R_1, and H with the number of stacking (n), for Configuration 2 is performed and curve fit equation is provided to represent the variation of these variables, which will be helpful for the designer in selecting the variables that provides optimum stiffness and load-carrying capacity of a stacked PMB. Figure 8(a) to (d) represents the plot of variables C, R_m, R_1, and H w.r.t. "n" for Configuration 2 for different R_4/H values, respectively.

From Figure 8(a) it can be observed that the variation of clearance for different R_4/H values is not substantial; however, from Figure 8(b) to (d), a considerable difference of values R_m, R_1, and H w.r.t. to R_4/H is noted. In the case of $R_4/H = 0.75$, a constant value of H is observed for different values of "n". The occurrence of constant values is due to the constraint provided in the optimization. Variation of the variables for different R_4/H values are investigated and curve fit equations are proposed for each variable as function of (i) "n" and (ii) variables value estimated at n=1. Further, ratio of first variable value (n=1) and nth value is estimated and their values for different $R_4/$

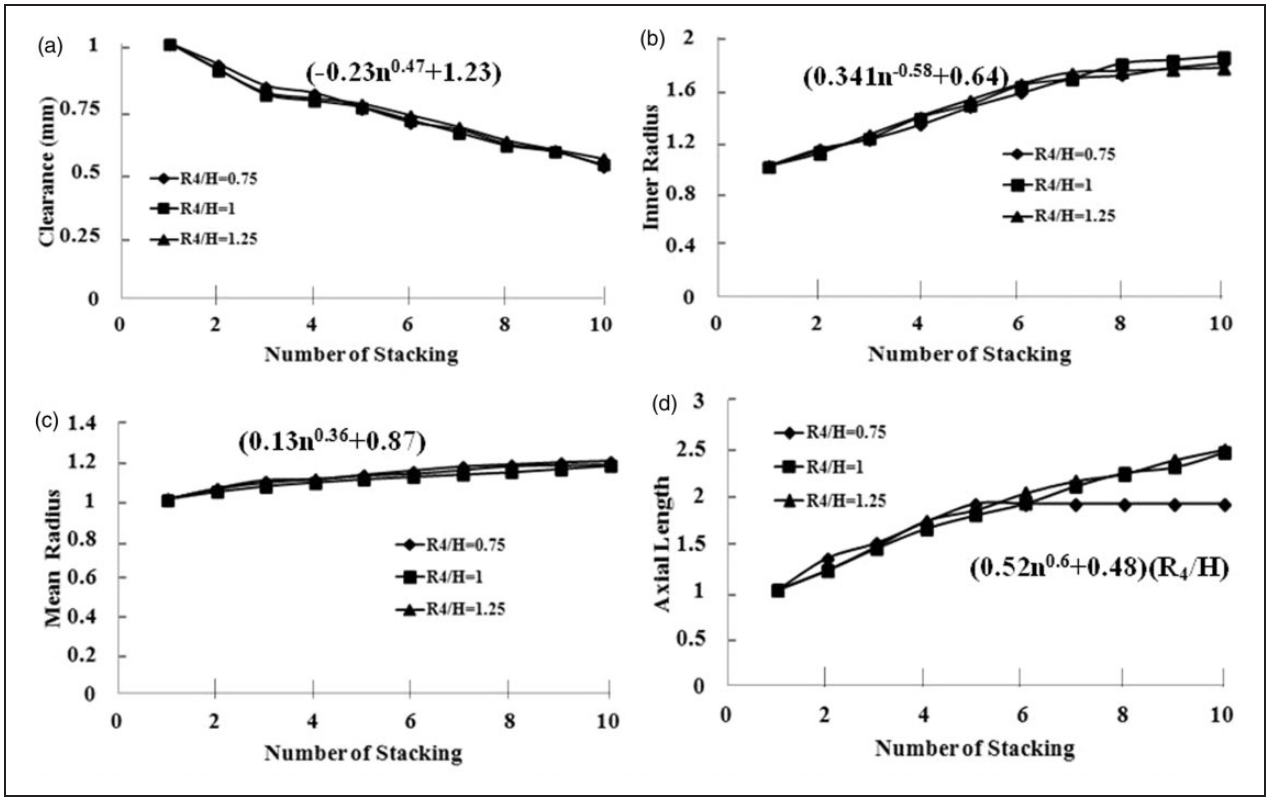

Figure 10. Variation of variables with the number of stacking and curve fit equation of Configuration 3 for different R_4/H values: (a) clearance, (b) mean radius, (c) inner radius, (d) axial length.

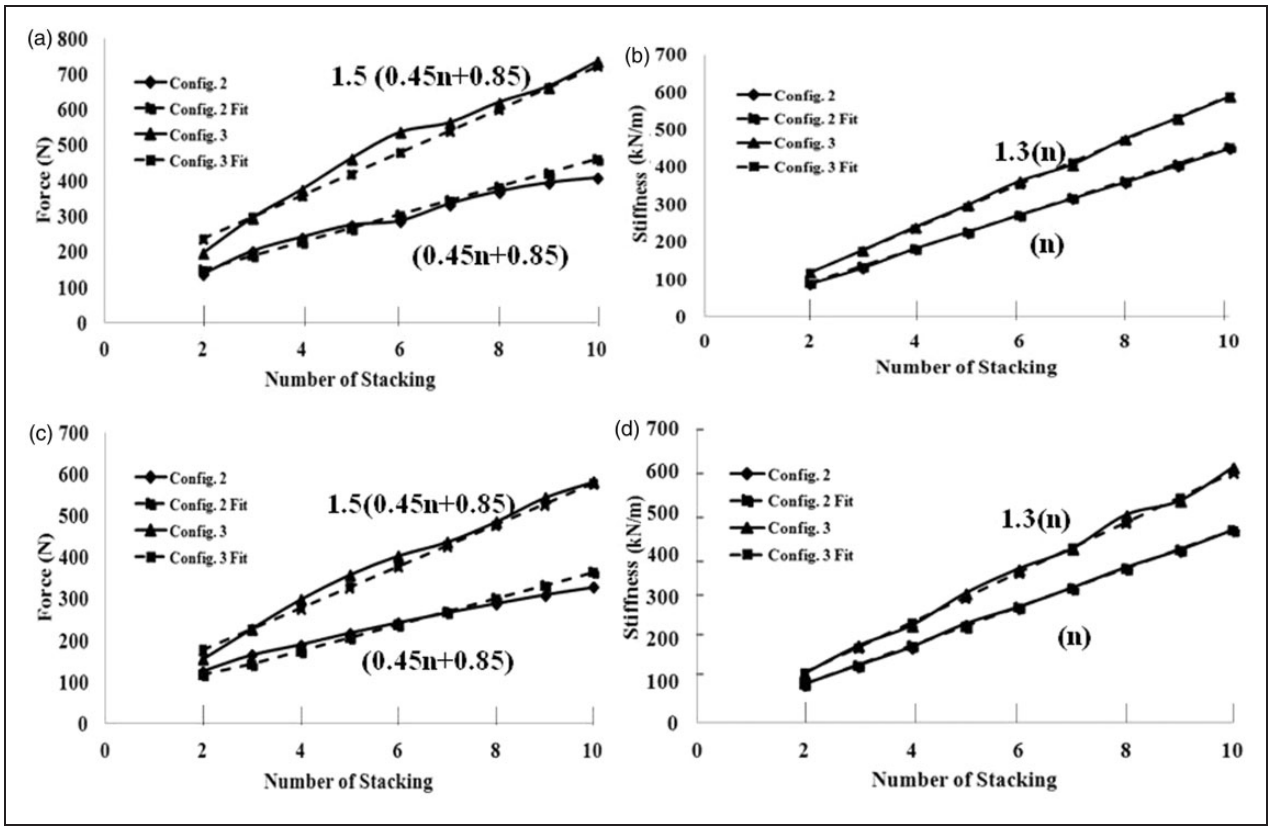

Figure 11. Force and stiffness of Configurations 2 and 3 for $R_4/H = 1$, $V = 1 \times 10^{-4}$ m^3 and 2×10^{-4} m^3: (a) force for $V = 1 \times 10^{-4}$ m^3, (b) stiffness $V = 1 \times 10^{-4}$ m^3, (c) force $V = 2 \times 10^{-4}$ m^3, (d) stiffness $V = 2 \times 10^{-4}$ m^3.

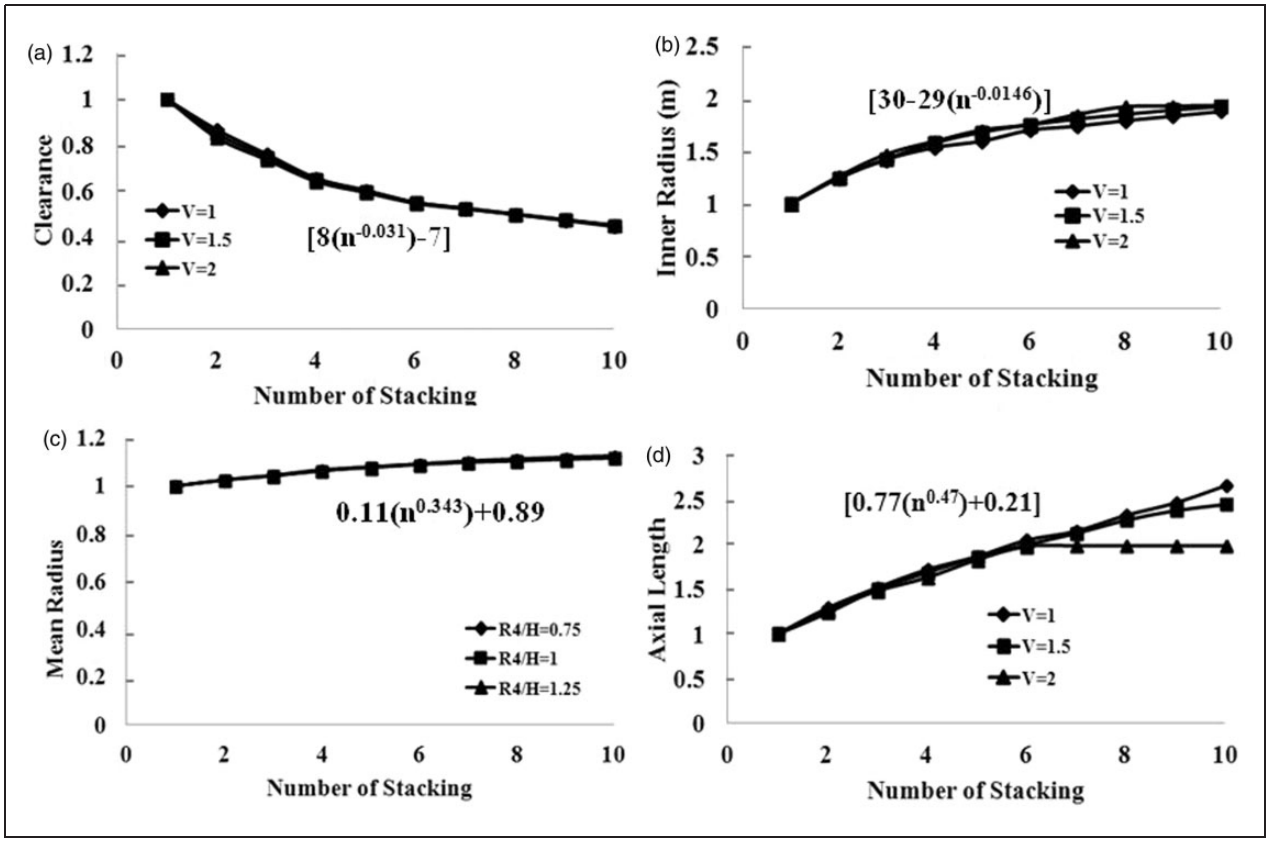

Figure 12. Variation in parameters with the number of stacking for Configuration 2 for different volumes: (a) clearance, (b) mean radius, (c) inner radius, (d) axial length.

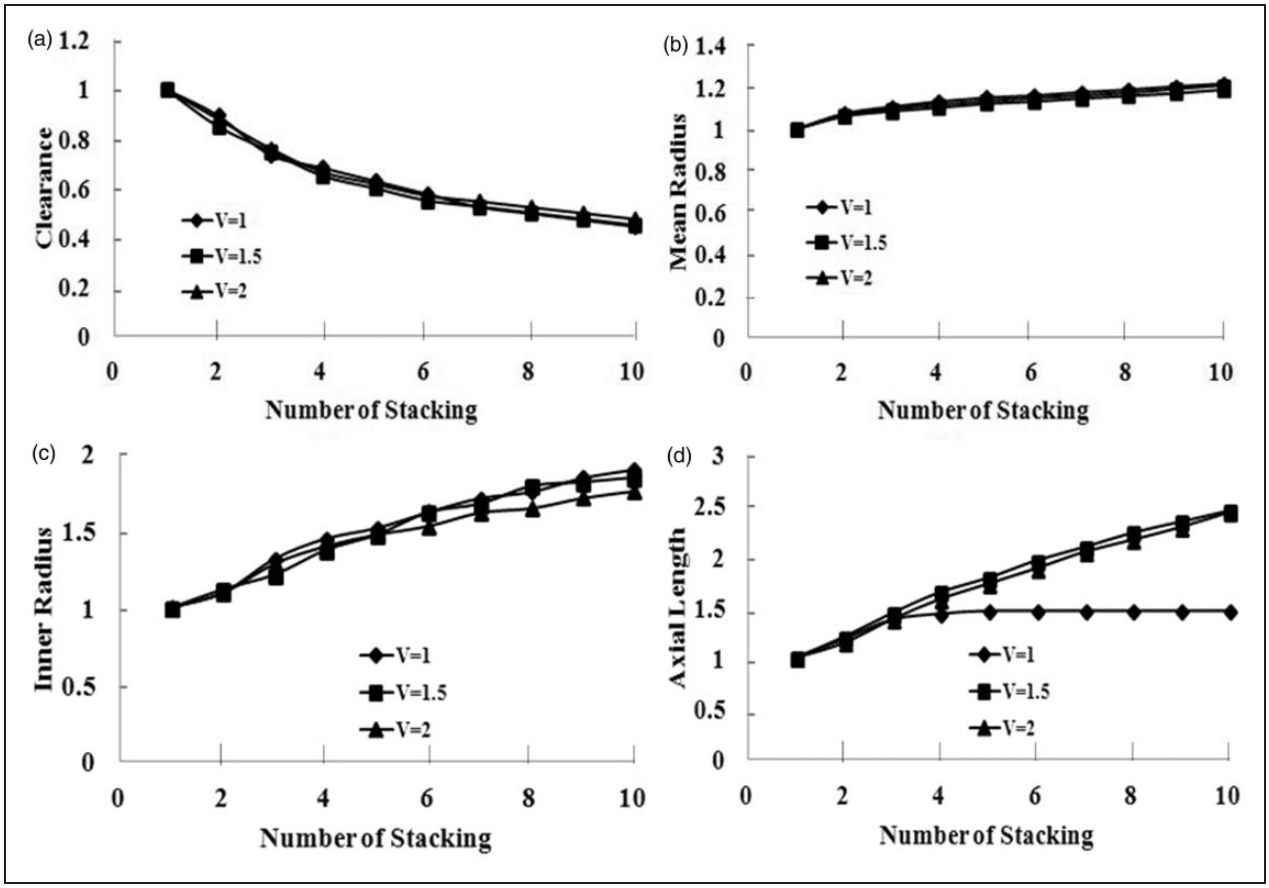

Figure 13. Variation in parameters with "*n*" for Configuration 3 and for different volumes using curve fit equations: (a) clearance, (b) mean radius, (c) inner radius, (d) axial length

Table 10. Curve fit equations for stiffness and force for different configurations and cases.

Config.	Case	Force	Stiffness
2	Maximizing load	$F_n = (7n-4)/(n+2)F_r$	$K_n = nK_r$
2	Maximizing stiffness	$F_n = nF_r$	$K_n = nK_r$
2	Maximizing both stiffness and load	$F_n = (0.45n + 0.9)F_r$	$K_n = nK_r$
3	Maximizing load	$F_n = 1.8\ (7n-4)/(n+2)F_r$	$K_n = 1.3nK_r$
3	Maximizing stiffness	$F_n = 1.3nF_r$	$K_n = 1.3nK_r$
3	Maximizing both stiffness and load	$F_n = k(0.45n + 0.9)F_r$	$K_n = 1.3nK_r$

Table 11. Dimension of PMB considered for validation.

	Dimensions of the PMB				
Ref.	R_1 (m)	R_2 (m)	R_3 (m)	R_4 (m)	H (m)
Mukhopadhyay et al.[7]	0.011	0.02	0.0245	0.0375	0.05

H values are plotted in Figure 9. It is interesting to observe from Figure 9(a) to (c) that the variation for variables C, R_m, and R_1 for different R_4/H values is the same and their curve fit equation is provided in equation (12a) to (12c), respectively. The curve fit equations are estimated by regression method provided by Lijesh and Hirani.[12]

$$C_n = \left[8\left(n^{-0.031}\right) - 7\right]C_r \tag{12a}$$

$$R_{1,n} = \left[30 - 29\left(n^{-0.0146}\right)\right]R_{1r} \tag{12b}$$

$$R_{m,n} = \left[0.1\left(n^{0.343}\right) + 0.89\right]R_{mr} \tag{12c}$$

$$H_n = \left[0.77\left(n^{0.47}\right) + 0.21\right](R_m/H)H_r \tag{12d}$$

In case H, the estimated values for different R_4/H values are different as depicted from Figure 9(d). However, by multiplying the value of R_4/H to each value of H, same values are noted. Due to constant values of H for $R_4/H = 0.75$, a straight line is seen (Figure 9(e)). The curve fit equation for H is provided in equation 12(d).

Similarly, variation of variables C, R_m, R_1, and H w.r.t "n" for different R_4/H values for Configuration 3 is studied and by following the above procedures, the plot and the curve fit equation estimated for variables C, R_m, R_1, and H is provided in Figure 10(a) to (d) and equation (13a) to (13d), respectively

$$R_1 = (0.341n^{0.58} + 0.64)R_{1,r} \tag{13a}$$

$$C = (-0.23n^{0.47} + 1.23)C_r \tag{13b}$$

$$R_m = (0.13n^{0.36} + 0.87)R_{m,r} \tag{13c}$$

$$H = (0.52n^{0.6} + 0.48)(R_m/H)H_r \tag{13d}$$

Multi-objective optimization considering different volumes

In the subsequent section, optimization is performed for different volumes (V), of PMBs: $1\times10^{-4}\,\mathrm{m}^3$ and $2\times10^{-4}\,\mathrm{m}^3$and for $R_4/H = 1$. The obtained values of load and stiffness for volume $V = 1\times10^{-4}\,\mathrm{m}^3$ is plotted in Figure 11(a) and (b), respectively and for $V = 2\times10^{-4}\,\mathrm{m}^3$ is plotted in Figure 11(c) and (d), respectively. It is interesting to note that equation fitting the optimization values for stiffness and load is the same as that of $V = 1.5\times10^{-4}$.

The obtained values of C, R_m, R_1, and H with curve fit equation are plotted in Figure 12(a) to (d). Unlike for different R_4/H values, the values of H did not vary with volume. Further, in equations (12a) to (12c) for different R_4/H values will fit the estimated values for the present case as these equation fits the common value of $R_4/H = 1$ and $V = 1.5\times10^{-4}\,\mathrm{m}^3$. H value is not varying with volume and the new curve fit equation for H is provided in the following equation

$$H_n = \left[0.77(n^{0.47}) + 0.21\right]H_r \tag{14}$$

The obtained values of C, R_m, R_1, and H along with the obtained values from curve fit equation are plotted in Figure 13(a) to (d). Equations (13a) to (13c) for different R_4/H values will suit the estimated values for the present case. Since the value of H is not varying with volume the curve fit equation for H is provided in the following equation

$$H_n = (0.52n^{0.6} + 0.48)H_r \tag{15}$$

The curve fit equations for stiffness and force obtained for different optimization cases and configurations are consolidated and tabulated in Table 10 with curve fit equations for different variables. In this table, the value of $k = 3.6(R_4/H)^2 - 7.5(R_4/H) + 5.4$

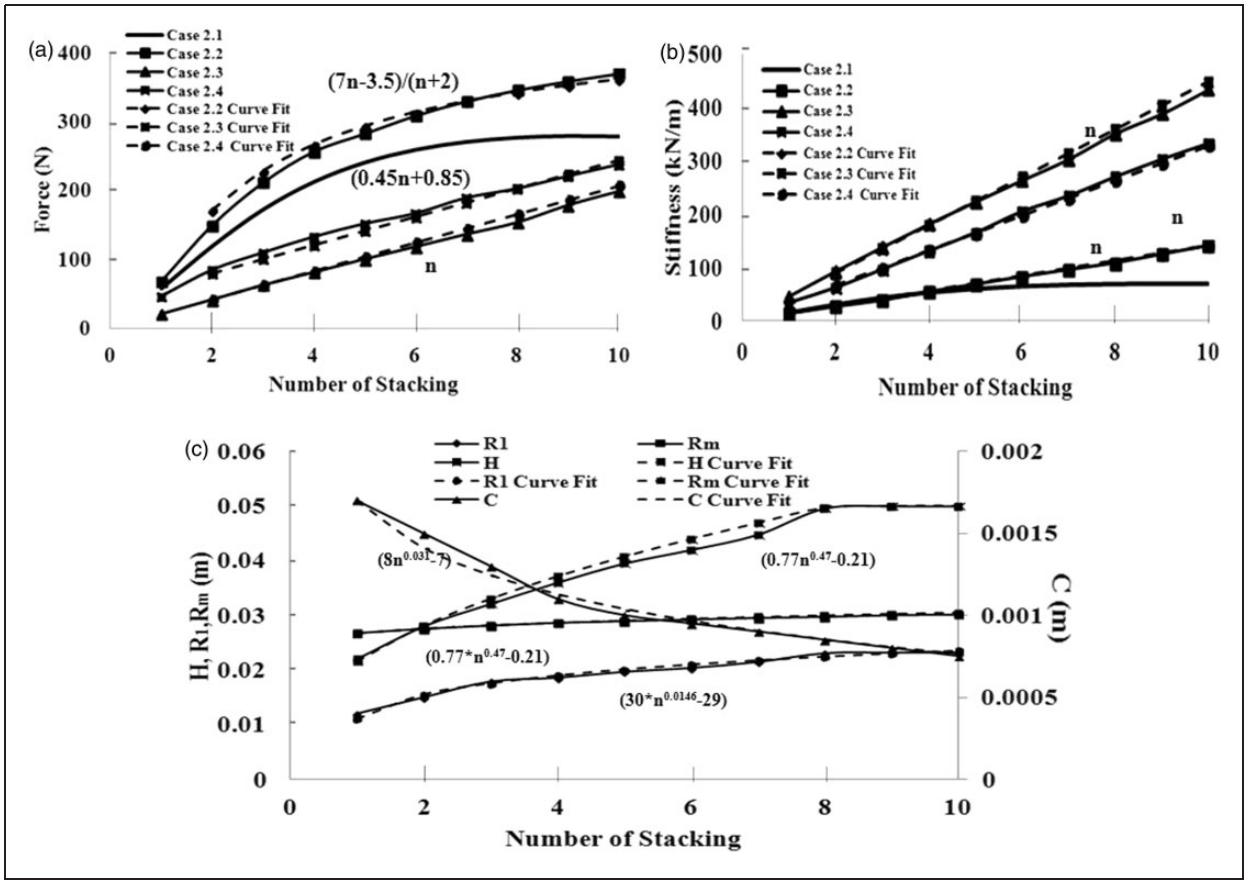

Figure 14. Estimated values of load and stiffness from optimization and their estimated curve fit equation for Case 2: (a) load, (b) stiffness, (c) estimated values of variables from optimization and curve fit equation.

Methodology to estimate load and stiffness

In this section, the methodology to be followed to estimate the values of load, stiffness, and variables are detailed. The steps to be followed are as follows:

Step 1: Estimate the values of load and stiffness for the Configuration 1 using equations (1) and (3) or by using analytical equation provided by Lijesh and Hirani.[12]
Step 2: Estimate R_4/H
Step 3: Use equations (12) and (13) respectively to obtain values of variables (C, R_m, R_1, and H) for Configurations 2 and 3.
Step 4: Using Table 10, estimate the values of load and stiffness for Configurations 2 and 3.
Step 5: Using equations (12) and (14), estimate the values of variables for different R_4/H values, for Configuration 2. Similarly for Configuration 3, equations (13) and(15) has to be used to estimate the values of variables.

Validation of the proposed methodology

Validation and demonstration of the proposed methodology is dealt with for different cases by considering dimensions of PMBs from Mukhopadhyay et al.[7] in this section. The dimensions of the PMB considered are tabulated in Table 11.

Case 1: Load-carrying capacity and stiffness of PMB having Configuration 1 is estimated for (i) dimension of the bearing provided in Table 11, (ii) maximization of load, (iii) maximization of stiffness, and (iv) maximization of both load and stiffness. The force and stiffness values are estimated using equations (2) and (3). Further, these values can also be estimated using the analytical equation provided by Lijesh and Hirani.[12] The details and the obtained results in each case are summarized below.

Case 1.1: Load and stiffness values for the provided dimensions of the bearing are estimated to be 56.9 N and 14.5 kN/m. The eccentricity ratio is set to be 0.9 and the magnetic remanence values for both stator and rotor is considered to be 1 T.

Case 1.2: Single-objective optimization is performed for Configuration 1 to achieve maximum load-carrying capacity by providing constant and constraints provided in the section ''Single-objective optimization''. The estimated load and stiffness values are 65 N and 8.367 kN/m. As compared to Case 1.1, not much difference in the load-carrying capacity is observed; however, the stiffness value has reduced considerably.

Table 12. Estimated values of load from optimization and curve fit for different cases for Configuration 2.

					Curve fit							Curve fit			
n	Case 2.1 (N)	Case 2.2 (N)	Case 2.3 (N)	Case 2.4 (N)	Case 2.2 (N)	Case 2.3 (N)	Case 2.4 (N)	R_1 (m)	R_m (m)	R_4 (m)	C (m)	H (m)	R_1 (m)	R_m (m)	C (m)	H (m)
1	57	68	21	46	65	21	46	0.0120	0.0268	0.035	0.00170	0.0220	0.0110	0.0268	0.00170	0.0216
2	119	149	41	84	114	41	80	0.0150	0.0276	0.035	0.00150	0.0280	0.0155	0.0276	0.00141	0.0281
3	172	211	63	109	143	62	100	0.0179	0.0282	0.035	0.00130	0.0321	0.0175	0.0282	0.00124	0.0330
4	212	256	81	132	172	82	121	0.0186	0.0287	0.035	0.00110	0.0360	0.0190	0.0286	0.00113	0.0371
5	240	282	100	151	202	103	141	0.0197	0.0290	0.035	0.00100	0.0395	0.0201	0.0290	0.00104	0.0407
6	259	308	118	166	231	124	162	0.0204	0.0293	0.035	0.00095	0.0420	0.0210	0.0294	0.00097	0.0439
7	270	329	136	189	260	144	182	0.0215	0.0296	0.035	0.00090	0.0448	0.0217	0.0297	0.00090	0.0469
8	277	345	153	202	286	165	203	0.0231	0.0298	0.035	0.00085	0.0496	0.0224	0.0300	0.00085	0.0496
9	279	358	178	220	319	185	223	0.0232	0.0301	0.035	0.00080	0.0500	0.0230	0.0302	0.00080	0.0500
10	278	369	198	237	348	206	244	0.0232	0.0302	0.035	0.00075	0.0500	0.0235	0.0305	0.00076	0.0500

Case 1.3: Single-objective optimization is performed for Configuration 1 to achieve maximum stiffness. The estimated load and stiffness values are 5 N and 28.837 kN/m. It can be observed that as compared to Cases 1.1 and 1.2, the load-carrying capacity has reduced while considerable increase in stiffness is noted.

Case 1.4: Multi-objective optimization is performed for maximizing load and stiffness in a constant volume of $1 \times 10^{-4}\,m^3$. The obtained load and stiffness values are 45.6 N and 29.56 kN. Multi-objective optimization shall provide good load-carrying capacity and stiffness values for PMB compared to other cases.

Case 2: Load-carrying capacity and stiffness of stacked PMB having Configuration 2 is estimated. For this, the axial length is divided into 2 to 10 sections and the load and stiffness is calculated. This case is divided into four cases further: (i) by considering dimension of the bearing provided in Table 10 and division of H in 2 to 10 sections, (ii) for maximization of load, (iii) for maximization of stiffness, and (iv) maximization of both load and stiffness considering constant volume. The results obtained are detailed below:

Case 2.1: In this case, H is divided by 2 to 10 and obtained values of load and stiffness is plotted in Figure 14(a) and (b), respectively. From this figure, it can be observed that the values of load and stiffness got saturated after $n = 5$.

Case 2.2: Single-objective optimization for achieving maximum load-carrying capacity of Configurations 2 is conducted. The estimated load and stiffness values are plotted in Figure 14(a) and (b), respectively. The value of stiffness is linearly increasing. In comparison with Case 2.1, increase in both load-carrying capacity and stiffness is observed after n=5. Further the curve fit equation fitting the load and stiffness values is estimated to be $F_n = (7n-3.5)/(n+2)F_r$ and $K_n = nK_r$, which is the same as that of equation provided in Table 10. The values obtained from optimization and curve fit equation is plotted in Figure 14(a) and (b).

Case 2.3: Optimization is performed for achieving maximum stiffness and the estimated load and stiffness values are plotted in Figure 14(a) and (b). Comparing Case 2.1 and Case 2.2, considerable reduction in load and increase in stiffness is observed. The equation fitting load and stiffness values are estimated to be $F_n = nF_r$ and $K_n = nK_r$, which is similar to the equation provided in Table 10. The values obtained from optimization and curve fit equation for load and stiffness for the current case is plotted in Figure 14(a) and (b).

Case 2.4: Multi-objective optimization is performed for achieving higher load and stiffness, without compromising on each other's values. The obtained values of load and stiffness is plotted in the same Figure 14(a) and (b), respectively. From these

Table 13. Estimated values of stiffness from optimization and curve fit for different cases of Configuration 2.

n	Case 2.1	Case 2.2	Case 2.3	Case 2.4	Case 2.2 Curve fit	Case 2.3 Curve fit	Case 2.4 Curve fit
1	14,052	14,000	44,837	32,863	14,000	44,837	32,863
2	29,282	27,642	92,021	61,281	28,000	89,674	65,726
3	42,453	39,148	137,100	95,797	42,000	134,511	98,589
4	52,395	55,171	180,510	130,630	56,000	179,348	131,452
5	59,352	68,976	222,370	164,580	70,000	224,185	164,315
6	63,955	83,114	262,550	204,930	84,000	269,022	197,178
7	66,766	96,152	302,210	234,310	98,000	313,859	230,041
8	68,300	108,630	350,330	270,350	112,000	358,696	262,904
9	68,885	124,875	387,330	303,320	126,000	403,533	295,767
10	68,703	140,650	432,800	333,040	140,000	448,370	328,630

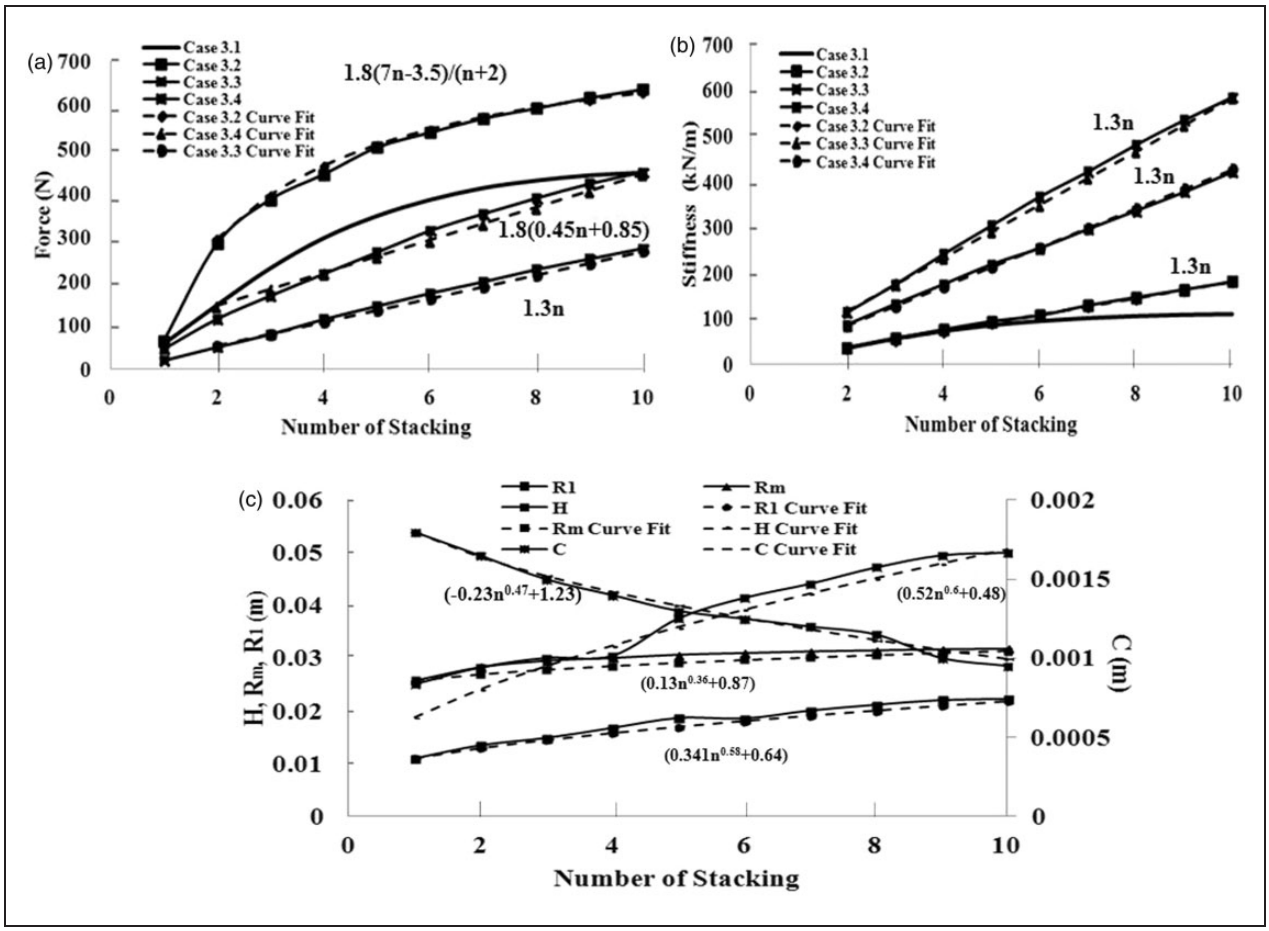

Figure 15. Estimated values of load stiffness and variables from optimization for Case 3: (a) load, (b) stiffness, (c) estimated values of variables from optimization and curve fit equation.

figure, it can be observed that the value of loads and stiffness for this case is between the results obtained from Cases 2.2 and 2.3. The curve fit equation estimated for variation of load and stiffness is $F_n = (0.45n + 0.85)F_r$ and $K_n = nK_r$, which is similar to the equation provided in Table 10. The values obtained from optimization and curve fit equation for load and stiffness for this case are presented in Figure 14(a) and (b).

The estimation of the variables from multi-objective optimization and curve fit equation provided in equation (12) is plotted in Figure 14(c). From this figure, it can

Table 14. Estimated values of load from optimization and curve fit for different cases for Configuration 3.

n	Case 3.1 (N)	Case 3.2 (N)	Case 3.3 (N)	Case 3.4 (N)	Curve fit											
					Case 3.2 (N)	Case 3.3 (N)	Case 3.4 (N)	R_1 (m)	R_m (m)	R_4 (m)	C (m)	H (m)	R_1 (m)	R_m (m)	C (m)	H (m)
2	145	286	51	114	165	298	145	0.0135	0.0283	0.0350	0.00165	0.0282	0.0155	0.0276	0.00164	0.0241
3	229	386	80	167	221	397	182	0.0149	0.0295	0.0350	0.00150	0.0300	0.0175	0.0282	0.00152	0.0285
4	298	443	114	216	257	463	219	0.0168	0.0300	0.0350	0.00140	0.0304	0.0190	0.0286	0.00142	0.0324
5	348	504	144	266	284	510	257	0.0187	0.0306	0.0350	0.00130	0.0375	0.0201	0.0290	0.00133	0.0359
6	385	538	173	315	303	546	294	0.0186	0.0309	0.0350	0.00125	0.0414	0.0210	0.0294	0.00125	0.0391
7	412	570	199	353	319	573	331	0.0201	0.0312	0.0350	0.00120	0.0441	0.0217	0.0297	0.00118	0.0422
8	429	593	227	389	331	595	368	0.0212	0.0314	0.0350	0.00115	0.0472	0.0224	0.0300	0.00111	0.0451
9	441	617	251	422	341	613	406	0.0221	0.0316	0.0350	0.00100	0.0495	0.0230	0.0302	0.00105	0.0479
10	447	636	275	448	349	628	443	0.0223	0.0317	0.0350	0.00095	0.0500	0.0235	0.0305	0.00099	0.0506

be inferred that, the provided curve fit equation is able to estimate the variation of variable precisely. The estimated values of load and stiffness from optimization and curve fit equation for different cases in Configuration 2 are listed in Tables 12 and 13, respectively.

Case 3: Load-carrying capacity and stiffness of stacked PMB having Configuration 3 is estimated. Methodology used for in Case 2 is followed for the present case. The results obtained for different cases are detailed below:

Case 3.1: H is divided by 2 to 10 and obtained values of load and stiffness are plotted in Figure 15(a) and (b), respectively. From these figures, it can be observed that the values of load and stiffness did not increase linearly with the number of stacking.

Case 3.2: Single-objective optimization for achieving maximum load-carrying capacity of Configurations 3 is performed. The estimated load and stiffness values are plotted in Figure 15(a) and (b), respectively. The value of stiffness is linearly increasing. Comparing Case 3.1, considerable increase in the load-carrying capacity and meagre increase in stiffness is noted. Further the curve fit equation, fitting the load and stiffness values is estimated to be $F_n = 1.8(7n-3.5)/(n+2)F_r$ and $K_n = 1.3nK_r$, which is same as that of equation provided in Table 10. The values obtained from optimization and curve fit equation for load and stiffness is plotted in Figure 15(a) and (b).

Case 3.3: Optimization is performed for achieving maximum stiffness and the estimated load and stiffness values are plotted in Figure 15(a) and (b). Comparing Cases 3.1 and 3.2, considerable reduction in load and increase in stiffness is observed. The equation fitting the load and stiffness values are estimated to be $F_n = 1.3(0.45n + 0.85)$ and $K_n = 1.3nK_r$, which is same as that of the equation provided in Table10. The values obtained from optimization and curve fit equation for load and stiffness for this case is plotted in Figure 15(a) and (b).

Case 3.4: The obtained values of load and stiffness after performing multi-objective optimization is plotted in the same Figure 15(a) and (b), respectively. From these figures, it can be observed that the value of loads and stiffness for this case is between case 3.2 and 3.3. The curve fit equation estimated for variation of load and stiffness is $F_n = 1.8(0.45n + 0.85)F_r$ and $K_n = 1.3nK_r$, which is provided in Table 10. The values obtained from optimization and curve fit equation for load and stiffness for this case is plotted in Figure 15(a) and (b).

The estimated variables values from multi-objective optimization and curve fit equation (13) are plotted in Figure 15(c). From this figure, it can also be inferred that the provided curve fit equation is able to estimate the variation of the variable. The estimated values of load and stiffness from optimization and curve fit equation for different cases in Configuration 3 are provided in Tables 14 and 15, respectively.

Table 15. Estimated values of stiffness from optimization and curve fit for different cases of Configuration 3.

n	Case 3.1	Case 3.2	Case 3.3	Case 3.4	Case 3.2 Curve fit	Case 3.3 Curve fit	Case 3.4 Curve fit
2	35,867	37,114.88	114,538	86,584.52	36,400	116,576.2	85,443.8
3	56,786	57,484.63	175,621.2	131,817.1	54,600	174,864.3	128,165.7
4	73,497	76,809.04	242,158	175,162	72,800	233,152.4	170,887.6
5	86,067	94,779.71	304,680.8	219,062.2	91,000	291,440.5	213,609.5
6	95,225	107,591.7	367,631.6	254,765.7	109,200	349,728.6	256,331.4
7	101,680	129,619.4	422,383.1	296,605.5	127,400	408,016.7	299,053.3
8	106,080	147,289.8	481,357.8	337,319.3	145,600	466,304.8	341,775.2
9	108,900	164,337.9	535,262.7	378,337.2	163,800	524,592.9	384,497.1
10	110,400	181,358.1	585,440.7	422,519	182,000	582,881	427,219

Conclusion

Load and stiffness being contradicting parameters in optimization of PMBs, optimization based on multi-objective function with single objective to achieve both maximum load and stiffness is presented. The radial load and stiffness of the PMBs are estimated using 3D Coulombian equations. The presented optimization is based on the constraints, constants and bounds of the dimensions obtained from the data available in literatures.

Single- and multi-objective optimization is performed for three different PMB configurations: (i) mono-layer, (ii) conventional and (iii) RMD. For carrying out the single-objective optimization three different cases, maximizing load (Case 1), maximizing stiffness (Case 2), and minimizing volume (Case 3) are considered. From the optimization (single and multi-objective) results, following conclusions are presented:

- Single-objective optimization considering Case 1, has resulted in decrease in stiffness and vice versa for Case 2.
- Multi-objective optimization for maximizing load and stiffness has yielded values between Case 1 and Case 2.

Further, increase in load and stiffness with the number of stacking is investigated for different configurations and cases. It is observed that stiffness and load are increased linearly and nonlinearly respectively with the number of stacking. In the case of multi-objective optimization, variation of variables: C, R_m, R_1, and H with respect to n is studied. For designer's ease, equations representing load, stiffness, and the variation of each variable as a function of n are proposed. Using the dimensions of PMB from a published literature, it is demonstrated that the proposed equation is capable of predicting the variation in load, stiffness, and variables precisely, which might help in designing effective and efficient PMB.

Declaration of Conflicting Interests

The author(s) declared no potential conflicts of interest with respect to the research, authorship, and/or publication of this article.

Funding

The author(s) received no financial support for the research, authorship, and/or publication of this article.

References

1. Sun J, Ju Z, Han W, et al. A novel integrated 4-DOF radial hybrid magnetic bearing for MSCMG. *J Magnet Magnet Mater* 2017; 421: 86–97.
2. Kanemistu Y and Shirao Y. Turbo molecular pump. US Patent1992, 5152679.
3. Kimman MH, Langen HH and Munning Schmidt RH. A miniature milling spindle with active magnetic bearings. *Mechatronics* 2010; 20: 224–235.
4. Kumbernuss J, Jian C, Wang J, et al. A novel magnetic levitated bearing system for Vertical Axis Wind Turbines (VAWT). *Appl Energy* 2012; 90: 148–153.
5. Ren Y and Fang JC. High-precision and strong-robustness control for an MSCMG based on modal separation and rotation motion decoupling strategy. *IEEE Trans Ind Electron* 2014; 61: 1539–1551.
6. Tang EQ and Han BC. Design and implementation of a fault-tolerant magnetic bearing system for MSCMG. *Math Prob Eng* 2013; 2013: 12.
7. Mukhopadhyay SC, Ohji T and Iwahara M. Modeling and control of a new horizontal-shaft hybrid-type magnetic bearing. *IEEE Trans Ind Electr* 2000; 47: 100–108.
8. Paden B, Groom N and Antaki JF. Design formulas for permanent-magnet bearings. *J Mech Des* 2003; 125: 734–738.
9. Yonnet JP, Lemarquand G, Hemmerlin S, et al. Stacked structures of passive magnetic bearings. *J Appl Phys* 1991; 70: 6633–6635.
10. Bekinal SI and Jana S. Generalized three-dimensional mathematical models for force and stiffness in axially, radially, and perpendicularly magnetized passive magnetic bearings with 'n' number of ring pairs. *J Tribol* 2016; 138: 31105.

11. Moser R, Sandtner J and Bleuler H. Optimization of repulsive passive magnetic bearings. *IEEE Trans Magn* 2006; 42: 2038–2042.
12. Lijesh KP and Hirani H. Development of analytical equations for design and optimization of axially polarized radial passive magnetic bearing. *J Tribol* 2016; 137: 1–9.
13. Ravaud R, Lemarquand G and Lemarquand V. Force and stiffness of passive magnetic bearings using permanent magnets. Part 1: Axial magnetization. *IEEE Trans Magn* 2009; 45: 2996–3002.
14. Morales W, Fusaro R and Kascak A. Permanent magnetic bearing for spacecraft applications. *Tribol Trans* 2003; 46: 460–464.
15. Lijesh KP and Hirani H. Stiffness and damping coefficients for rubber mounted hybrid bearing. *Lubr Sci* 2014; 26: 301–314.
16. Tan Q, Li W and Liu B. Investigations on a permanent magnetic–hydrodynamic hybrid journal bearing. *Tribol Int* 2002; 35: 443–448.
17. Samanta P and Hirani H. Magnetic bearing configurations: Theoretical and experimental studies. *IEEE Trans Magn* 2008; 44: 292–300.
18. Lijesh KP and Hirani H. Magnetic bearing using rotation magnetized direction configuration. *J Tribol* 2015; 137: 1–11.
19. Wang FX, Wang JQ, Kong ZG, et al. Radial and axial force calculation of BLDC motor with passive magnetic bearing. No. 59977014, pp.290–293.
20. Byrd Richard H, Jean CG and Jorge N. A trust region method based on interior point techniques for nonlinear programming. *Math Prog* 2000; 89: 149–185.

Appendix

Notation

B	length of rotor magnet (m)
Br_1	magnetic remanence of stator (T)
Br_2	magnetic remanence of rotor (T)
C	radial clearance (m)
e	eccentricity (m)
$F_{y,s}$	radial force between two sector magnets (N)
$F_{y,a}$	radial load exerted by single-layer magnet (N)
$F_{y,CON}$	radial load exerted by conventional stacked PMB (N)
$F_{y,RMD}$	radial load exerted by RMD configured PMB (N)
F_n	estimated nth force
Fun	function
H	total length of stator (m)
L	axial length stacked ring (m)
K_n	estimated nth stiffness
n	number of stacking
r_{12},r_{34}	position vector (m)
R_C	R_m/C
R_L	R_m/L
R_m	mean radius (m)
R_1	inner radius of rotor magnet (m)
R_2	outer radius of rotor magnet (m)
R_3	inner radius of stator magnet (m)
R_4	outer radius of stator magnet (m)
Vol.	volume (m^3)
z_a	axial offset (m)
ε	eccentricity ratio
μ_0	permeability of air
θ	angle subtend by rotor magnet (rad)
θ'	angle subtend by stator magnet (rad)

Suffix

a	mono layer magnet
CON	conventional
k	number of stacking of magnetic ring for RMD PMBs
m	number of stacking of magnetic ring for conventional PMBs
p	perpendicular
RMD	rotational magnetization direction
y	y direction